JOURNAL OF PROPULSION AND POWER
Vol. 21, No. 6, November–December 2005

Primary Pollutant Prediction from Integrated Thermofluid–Kinetic Pulse Combustor Models

H. M. Heravi*
Azad University, 91735 Mashhad, Iran
J. R. Dawson†
University of Cambridge, Cambridge, England CB2 1PZ, United Kingdom
and
P. J. Bowen‡ and N. Syred‡
Cardiff University, Cardiff, Wales CF24 0YF, United Kingdom

A phenomenological model for pulsating combustion by predicting characteristics of primary pollutants NO_x and CO, as well as minor combustion species via integration with a detailed kinetic mechanism (GRI-Mech2.11) and a reduced kinetic model, both derived from the CHEMKIN suite is studied with the aim of improvement. Homogeneous methane–air mixtures have been modeled across a range of practical, fuel-lean operating conditions, and predictions of primary pollutants from both models have been compared with available data. The use of a more realistic oscillatory Nusselt number is necessary to provide agreement with the experimental finding of relative insensitivity of primary pollutant emissions to input power. Oscillatory characteristics of combustion species are generated and are consistent with published data. Optimum operating conditions of the combustor are predicted to be around an equivalence ratio of 0.74, where NO_x and CO emissions of only a few parts per million occur. NO_x and CO predictions using the reduced mechanism provide better agreement with experimental data than those using GRI-Mech2.11. This probably results from the construction of the reduced model from the detailed mechanisms in GRI Mech3.

Nomenclature

A_e = tailpipe cross-sectional area, m^2
A_s = combustor surface area, m^2
A' = kinetic constant for fuel reaction rate, s
C_p = specific heat for constant pressure, J/kg · K
D_{tp} = diameter of the tailpipe, m
d_0 = diameter of the combustion chamber, m
f = friction factor
f^* = frequency of oscillation, Hz
h = heat transfer coefficient, $W/m^2 \cdot K$
L_{c2} = ratio of combustion zone volume to A_e, m
L_{tp} = ratio of combustion zone volume to A_s, m
Nu = Nusselt number for oscillatory flow
Nu_0 = Nusselt number for steady flow
R = gas constant, J/mol · K
S_r = stoichiometric mass ratio
T_e = temperature at the tailpipe entrance, K
T_w = wall temperature, K
T_0 = ambient temperature, K
$\tilde{T}$ = temperature normalized with ambient
$\tilde{T}_a$ = dimensionless activation temperature
t = time, s
$\tilde{u}$ = normalized gas velocity in the tailpipe
V = combustion chamber volume, m^3
Y_f = fuel mass fraction in combustion chamber
$Y_{f,i}$ = inlet fuel mass fraction
Y_0 = O_2 mass fraction in combustion chamber
$Y_{0,e}$ = exit oxygen mass fraction
$Y_{0,i}$ = inlet oxygen mass fraction
Z_e = exit mass flow per combustion zone volume
γ = ratio of specific heats
ΔH_f = heat of reaction, J/kg
λ = wavelength of oscillation, m
μ = dynamic viscosity of gas, kg/ms
ρ_0 = ambient density, kg/m^3
τ_c = combustion time, s
τ_f = flow time, s
τ_{HT} = heat transfer time, s
ϕ = equivalence ratio

Received 8 September 2004; revision received 22 February 2005; accepted for publication 8 March 2005.

*Assistant Lecturer, Department of Mechanical Engineering.
†Research Associate and College Lecturer in Engineering, New Hall, Department of Engineering, Trumpington Street.
‡Professor, Institute of Sustainability, Energy and Environmental Management Cardiff School of Engineering, The Parade. Member AIAA.

I. Introduction

FLAMES are sensitive to excitation from sound waves, with their response dependent on the amplitude, frequency, and nature of acoustic wave impingement. In the Helmholtz pulse combustor, the response to this excitation leads to an increased rate of combustion and thermal efficiency, with associated high rates of heat transfer and reduced pollutant emissions under suitable operating conditions.[1–5] The aim of this research program is to further develop an integrated phenomenological thermofluid/chemical kinetic model,[6–10] by exploring the effect of detailed chemical kinetic schemes employed ranging from a reduced mechanism (17 reactions)[9] to the developed GRI-Mech2.11 scheme (279 reactions)[11] and appraising predictions against published experimental data.

The type of pulse combustor considered belongs to the aerovalved family, the generic operation of which is nonpremixed but has the added practical attraction of providing self-sustaining operation with no mechanical moving parts. Whereas predictions of NO_x production due to forced oscillations of the pressure, velocity, and heat release within the combustor have been presented previously,[4] the novelty of the current approach is that no pulsations are presumed a priori; transient oscillations have been shown to be a natural solution of the simplified first-order coupled time-dependent problem.[6] Hence the time-dependent NO_x predictions are governed simply by the boundary conditions of the model. A simplified model facilitates

numerical experiments capable of isolating and investigating the mechanisms that contribute to reduced NO_x and CO performance in pulse combustors compared to experimental combustors.

The interrelation between the physics and chemistry that govern the operation of pulse combustors is complex and involves complex fluid flows with associated mixing issues, chemical kinetics, turbulent combustion, heat transfer, thermoacoustic coupling, etc. Although three-dimensional transient computational fluid dynamics (CFD) combustion models are under development, they are at the moment too cumbersome and slow for most practical purposes. The role of the simplified phenomenological model is in providing relatively fast predictions and a transparency that allows scientific interpretation of predictions. Here the transient nature of operation is afforded higher priority than spatial variations; hence, this model provides spatially averaged, time-based predictions. The construction of a premixed version of the model has been described elsewhere.[7] This basic model was first improved to facilitate nonpremixed operation, more representative of aerovalved operation,[8] and then recently integrated with a reduced chemical kinetic scheme (using the CHEMKIN suite)[9] to provide the first predictions of primary pollutants NO_x and CO from this type of phenomenological model.[10] Here, the sensitivity of these predictions to the type of chemical kinetic scheme used are explored by generating and using a pulse-combustor model integrated with the GRI-Mech2.11 (Ref. 11) scheme for methane.

II. Previous Experimental Studies

There is a noticeable dearth of experimental data in the literature concerning the emissions performance of well-tuned, efficient pulse combustors. There are also many contradicting reports regarding the influence of various geometrical parameters and loading on pollutant levels. As such, it is difficult to attribute general trends with either aerovalved or mechanically valved combustors or their types. The results reported in Refs. 2 and 12 were carried out with a premixed, mechanically valved Helmholtz-type pulse combustor and are currently the best available benchmark results. Other reports by Corliss et al.[13] and Barham et al.[14] have identified similar trends to the work of Keller and Hongo[2] and Keller et al.[12]

Keller and Hongo[2] derived NO_x generation rates operating with ϕ near to stoichiometric via cycle and spatially resolved temperatures and pressures. For ϕ near unity, the thermal NO_x mechanism dominates over prompt NO_x routes. In comparison with a comparable nonoscillatory combustor, a reduction in the average rates of NO_x formation was demonstrated. Lower average temperatures and residence times at high temperatures were considered to be the main mechanisms for this. Relevant subprocesses were considered to be: 1) recycling of previously exhausted products; 2) rapid mixing of the cooler fresh charge with hot combustion products, hence reducing residence time at high temperature; and 3) enhanced heat transfer at the combustor walls, considered the main effect.[2]

Further investigations[12] analyzed the effect of varying equivalence ratio and microscale mixing on CO and NO_x emissions; this was found to be independent of the microscale mixing processes employed for all equivalence ratios and also independent of fuel flow rate (power), which is contrary to previous predictions.[6–8] NO_x increased monotonically from a few parts per million at $\phi = 0.6$ to 35 ppm at $\phi \sim 1$. The CO trace showed a characteristic U shape, plateauing at $\phi \sim 0.75$, for $NO_x < 5$ ppm, before increasing again for $\phi \sim 1$. Prompt NO_x was considered the dominant production route under lean conditions, with thermal NO_x effectively switching off at $\phi = 0.76$.

Phase locked velocity measurements in the fuel and air inlet supply of a propane fired aerovalved pulse combustor operating at the lean limits[15] were shown to oscillate at the limit-cycle frequency. Thus, the instantaneous equivalence ratio varies throughout the limit cycle, though hovering for a significant part of the acoustic period between $\phi = 0.5$ and 0.6. Steady NO_x levels less than 30 ppm were measured during limit-cycle operation in the exhaust acoustic decoupler box. Modulation of the pressure time series was a notable feature, which induced cycle-to-cycle modulations.

III. Physical and Chemical Model Integration

The thermofluid model of the combustion chamber was originally based on the thermal model proposed by Richards et al.[6] and was previously modified to include separate oscillating air and fuel inlet characteristics.[8,16] A schematic of the model geometry is shown in Fig. 1. The model geometry, which determines the frequency characteristics, is based on an experimental aerovalved pulse combustor.[15] The transient, spatially averaged thermodynamic model is based on the energy equation within the combustor chamber control volume, coupled with a simple fluid dynamic submodel for the tail pipe. The model is described in detail elsewhere.[8,16] The model is akin to a perfectly stirred reactor, because a mixing timescale has not been incorporated, being dominated by chemical kinetics, though the importance mixing timescales is fully appreciated within the limits of aerovalved operation. The formulation of the original model,[6] developed from the energy balance, rendered it incapable of nonpremixed operation, also being only valid for near-stoichiometric conditions. For the improved model, equations for fuel and oxidant species as functions of time within the combustor are treated independently within the Runge–Kutta numerical solution scheme. Although not used here mixing timescales can be added to more accurately reflect the aerovalved process.

The main focus of this research has been to compare predictions, particularly predictions of primary pollutants, from the pulse combustor model integrated with a reduced chemical kinetic scheme, compared with those from a detailed kinetic mechanism. This is perceived to be one advantage of the phenomenological model over more detailed CFD models, in that its relative simplicity facilitates integration with chemical kinetic schemes of greater detail than is usually possible. The chemistry modeling has been undertaken using the commercially available CHEMKIN II (Ref. 17) package, more specifically, the SENKIN program. SENKIN predicts the time-dependent chemical kinetic behavior of a homogeneous gas-phase mixture in a closed system. This code is linked to the pulse combustor model at each time step to predict the mole fractions of the species, the flow chart is shown in Fig. 2. The reduced mechanism was based on the work of Sung et al.[9] and describes the methane oxidation chemistry in terms of 17 elementary reactions involving 21 species. The detailed mechanism employed via the GRI-Mech2.11

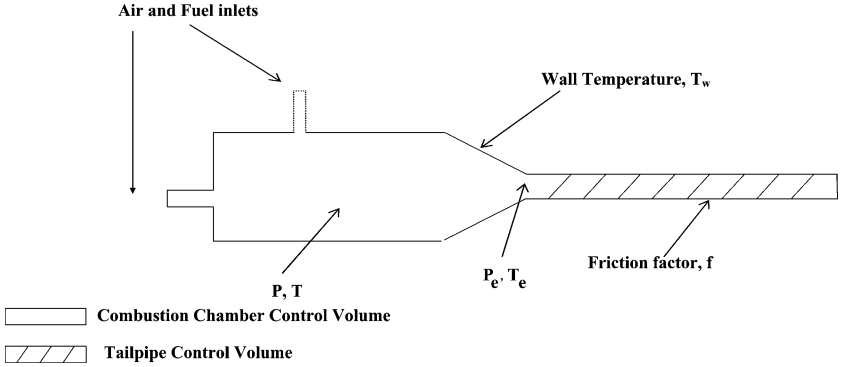

Fig. 1 Model control volume geometry.

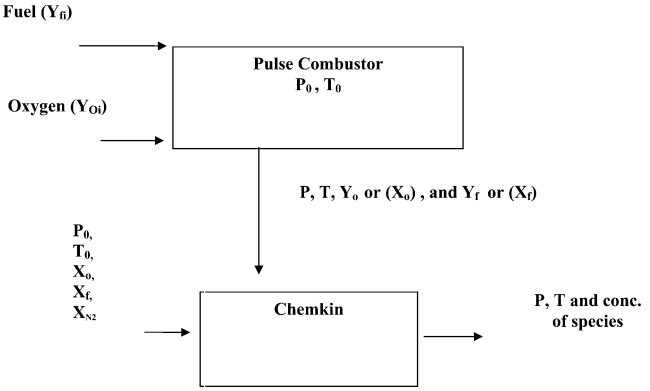

Fig. 2 Flow chart of integrated model linking of pulse combustor with CHEMKIN.

(Ref. 11) by comparison employs 49 species and 279 reactions. Thermodynamic properties used in this study were obtained from the CHEMKIN thermodynamic database.

The transient thermofluid results are presented in terms of the combustor pressure and temperature, and the chemical species predictions are presented in terms of primary reactants, CH_4 and O_2, primary combustion products, H_2O and CO_2, various influential minor chemical species, and the primary combustion pollutants, CO and NO_x. Results are presented for both the constant and oscillatory heat transfer, and the predictions are appraised against the time-averaged CO and NO_x predictions of Keller and Hongo[2] and Keller et al.[12]

A simple aerovalved pulse combustor can be modeled[8,16] via five normalized ordinary differential equations. The first differential equation describes the normalized temperature (thermal energy balance) over the combustion chamber,

$$\frac{d\tilde{T}}{dt} = \gamma\left\{\frac{1}{\tau_f}+\frac{1}{\tau_{HT}}+\frac{1}{\tau_c}\right\}\frac{\tilde{T}}{\tilde{P}} - \left\{(\gamma-1)\frac{Z_e}{\rho_0}+\frac{1}{\tau_f}+\frac{\gamma T_0}{\tau_{HT}T_w}\right\}\frac{\tilde{T}^2}{\tilde{P}} \tag{1}$$

where Z_c is the ratio of exit mass flow rate to the combustion chamber volume, τ_f is the characteristic flow time, τ_{HT} is the characteristic heat transfer time, and τ_c is the characteristic combustion time. Combining a mass balance with Eq. (1) results in an equation describing the time variation of the normalized pressure in the combustion chamber,

$$\frac{d\tilde{P}}{dt} = \gamma\left\{\frac{1}{\tau_f}+\frac{1}{\tau_{HT}}+\frac{1}{\tau_c}\right\} - \left\{\frac{Z_e}{\rho_0}+\frac{T_0}{\tau_{HT}T_w}\right\}\gamma\tilde{T} \tag{2}$$

To solve Eqs. (1) and (2), the characteristic combustion time in terms of instantaneous heat release per unit volume needs to be defined. Therefore, in addition to the total mass balance equations, one can write equations for the rate of change of the fuel and oxygen in the combustion chamber, respectively,

$$\frac{dY_f}{dt} = (Y_{f,i}-Y_f)\frac{\tilde{T}}{\tilde{P}}\frac{1}{\tau_f} + Y_f\frac{\tilde{T}}{\tilde{P}}\frac{Z_e}{\rho_0} - \frac{\tilde{T}}{\tilde{P}}\left(\frac{C_pT_0}{\Delta H_f}\right)\frac{1}{\tau_c} \tag{3}$$

$$\frac{dY_0}{dt} = (Y_{0,i}-Y_0)\frac{\tilde{T}}{\tilde{P}}\frac{1}{\tau_f} + Y_0\frac{\tilde{T}}{\tilde{P}}\frac{Z_e}{\rho_0} - Y_{0,e}\dot{m}_e\frac{\tilde{T}}{\tilde{P}}\frac{1}{\rho_0 V} - S_r\frac{\tilde{T}}{\tilde{P}}\left(\frac{C_pT_0}{\Delta H_f}\right)\frac{1}{\tau_c} \tag{4}$$

The momentum equation for the tailpipe in terms of the rate of tailpipe gas velocity (normalized to the cold flow tailpipe velocity) is required and defined as

$$\frac{d\tilde{u}}{dt} = (\tilde{P}_e-1)\left(\frac{RT_0\tau_f}{L_{tp}L_{c2}}\right)\frac{\tilde{T}_e}{\tilde{P}_e} - \frac{L_{c2}f}{2D_{tp}\tau_f}\frac{\tilde{u}^3}{|\tilde{u}|} \tag{5}$$

where

$$\tau_f = \rho_0/Z_i \tag{6}$$

is a characteristic flow time,

$$\tau_{HT} = L_{c1}\rho_0 C_p T_0/hT_w \tag{7}$$

is a characteristic heat transfer time, and

$$\tau_c = \rho_0 C_p T_0/\dot{Q} \tag{8}$$

is a characteristic combustion time.

Finally, the following equation to express the combustion time is derived by combining Eq. (7) with the heat release rate per unit area and fuel reaction rate for a single step reaction mechanism to solve Eqs. (3) and (4),

$$1/\tau_c = A'(\Delta H_f/C_pT_0)(\tilde{P}^{\,2}/\tilde{T}^{\,\frac{3}{2}})Y_f(Y_0/S_r)\exp(-\tilde{T}_a/\tilde{T}) \tag{9}$$

More detail and discussion of the model and its assumptions may be found elsewhere in the quoted Refs. 16 and 17. Another limitation of the previous model has been addressed by improving modeling of the heat transfer process in the oscillatory flowfield. Previous work employed a constant heat transfer coefficient $h = 120\ \mathrm{W/m^2\cdot K}$ to solve the characteristic heat transfer time in the combustion chamber control volume and was explored over a series of parametric studies.[6–8,16] An oscillatory Nusselt number is more appropriate when considering the physics underlying pulse combustor operation. An equation for expressing Nusselt number for a combustion chamber with lateral oscillations has been proposed previously[18] and has been incorporated into the pulse combustor model,

$$\mathrm{Nu}/\mathrm{Nu}_0 = 1 + 0.563\cdot \mathrm{Nu}_0^{-1}\cdot\left[\Delta P_0\big/2\mu f^*\right]^{0.65}\cdot[\mathrm{d}_0/\lambda] \tag{10}$$

Some trends, for example, the insensitivity of primary pollutant emissions to mass loading, can only be successfully modeled with the oscillatory Nusselt number. This is considered an important finding with regard to future pulse combustor model development.

IV. Results and Discussion

The extended system of equations is solved using the Runge–Kutta scheme for steady inlet conditions to determine whether the NO_x species balance results in a plausible limit-cycle solution within the combustor. Figures 3–5 show the time series of pressure and temperature oscillations and the pollutant mole fractions in the combustor section during transient startup and after steady conditions are established. In Figs. 3–5, the reduced mechanism is employed, the fuel supply is fixed at 0.57 g/s, $\phi = 0.85$, the Nusselt number is constant, and all pollutant predictions are corrected to 3% O_2. Figure 3 shows that the limit-cycle oscillations stabilize 100 ms after ignition, consistent with the previous models.[6–8] In this representative example, the resulting oscillation frequency is 71.5 Hz and shows good agreement with the operational frequency of the aerovalved combustor test facility on which the model dimensions are based.[15] The resulting pressure amplitudes are 12.2 kPa with a mean operating temperature of 1600 K. Comparison with Fig. 4 shows that pressure and temperature stabilize before the NO_x concentrations. This is due to the artificial conditions introduced at $t = 0$ s to invoke the reaction, resulting in unrealistically high NO_x production at these early stages. However, the NO_x species equation gradually

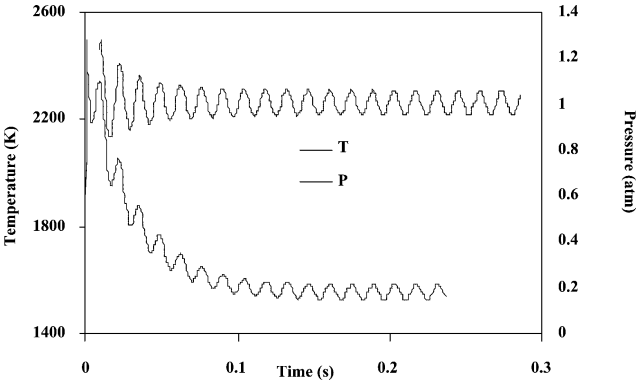

Fig. 3 Pressure and temperature for $\phi = 0.85$ using reduced scheme.

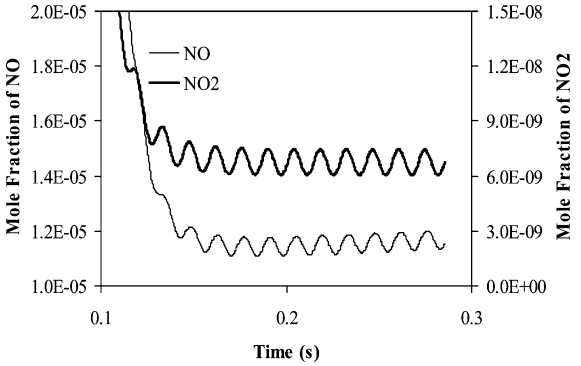

Fig. 4 NO_x mole fractions for $\phi = 0.85$ using reduced scheme.

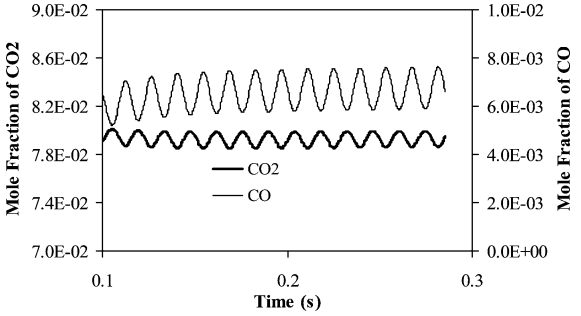

Fig. 5 CO and CO_2 mole fractions for $\phi = 0.85$ using reduced scheme in the combustor.

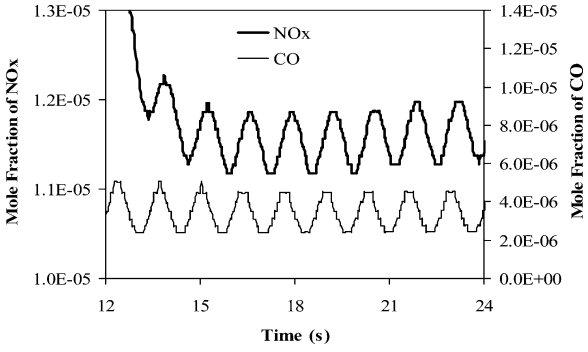

Fig. 6 NO_x and CO mole fractions for $\phi = 0.85$ near end of tailpipe using reduced mechanism.

purges the combustor, until limit-cycle oscillations are reached, with amplitudes about 20% of the mean. For this case, the mean concentration of NO and NO_2 is 11.7 and 0.07 ppm, respectively. NO_2 levels are, thus, negligible, and hereafter NO is used to represent the predicted NO_x value.

Combustor CO predictions approach 6000 ppm, reducing to ~4 ppm at the end of the tailpipe (Figs. 5 and 6); clearly the added fluid tailpipe residence time strongly influences predicted CO levels. Combustion chamber and tailpipe exit NO_x are very similar; thus, NO_x is unaffected by the tailpipe additional residence time. NO_x production is essentially constrained to the combustion chamber and combustion process.

The stabilized mean NO_x concentration of ~11 ppm agrees well with the literature[2,12,14,15] and indicates that the NO_x generation source term and species balance are satisfactorily integrated within the first-order coupled equation system and numerical scheme (Figs. 3–6). The NO_x levels generally oscillate in-phase with the predicted pressure and temperature oscillations, although closer inspection reveals a small phase shift ≈10 deg between NO_x and temperature while being almost precisely in-phase with pressure at this equivalence ratio.

With the ability of the integrated model to achieve stable NO_x oscillations, it is now possible to explore the influence of equivalence ratio on NO_x production within the lean range where prompt NO_x becomes the dominant formation mechanism, that is, $0.5 < \phi < 0.8$. To isolate the effect of equivalence ratio, parameters that have been found to influence NO_x production such as the heat transfer coefficient, wall temperature, and mass flow rate are kept constant.

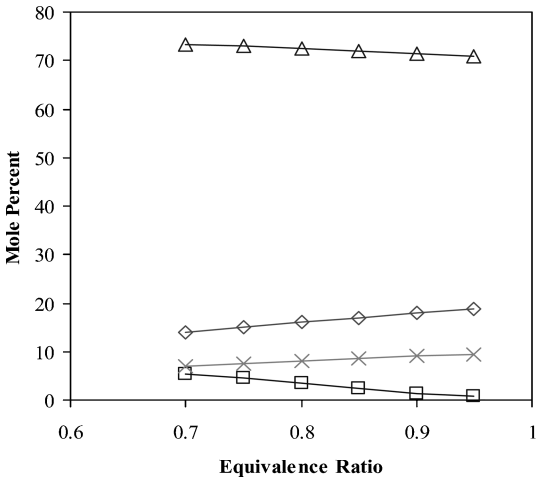

Fig. 7 Mole fraction of primary combustion products: □, O_2; ◇, H_2O; ×, CO_2; and △, N_2 for $\phi = 0.7$–0.95 (GRI-Mech2.11).

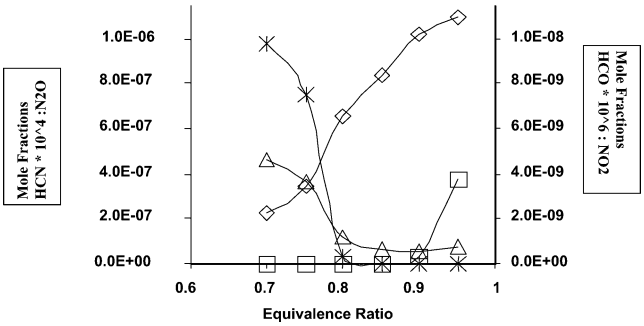

Fig. 8 Mole fraction of minor species: □, HCO; ×, HCN; △, N_2O; and ◇, NO_2 for $\phi = 0.75$–0.95 (GRI-Mech2.11).

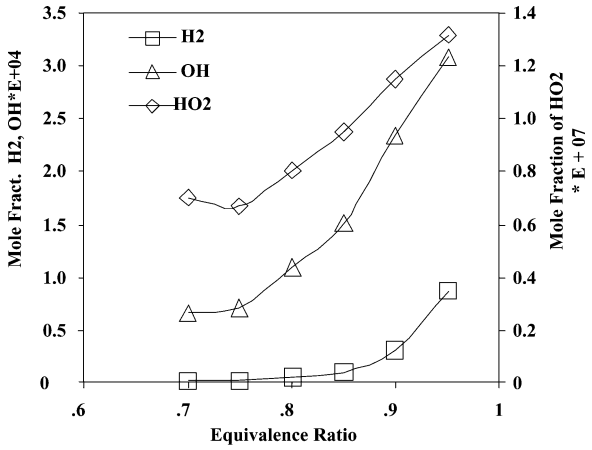

Fig. 9 Mole Fraction of minor species H_2, OH, and HO_2 from detailed kinetics.

The effects of changing the equivalence ratio on the primary combustion products of O_2, H_2O, CO_2, and N_2 using the detailed GRI-Mech2.11 (Ref. 11) scheme are shown in Fig. 7. Reassuringly, increase in the equivalence ratio from $\phi = 0.7$ toward stoichiometric conditions increases the production of CO_2 and H_2O and decreases the production of O_2, as expected from elementary combustion theory.

Figures 8 and 9 present the mean values of the oscillatory trends for the minor species across the range of equivalence ratios using the detailed kinetic scheme; they show a monotonic increase with

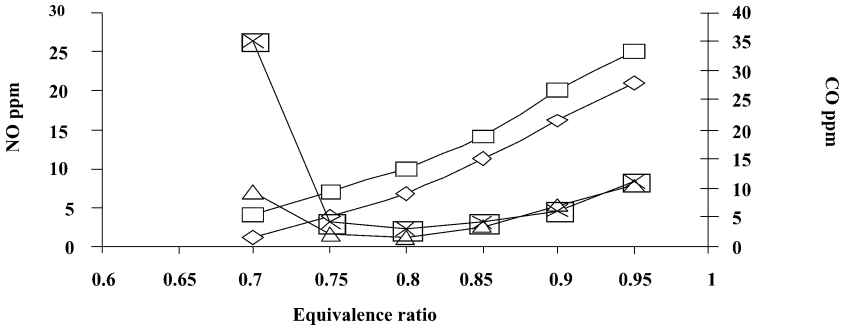

Fig. 10 Comparison of NO_x and CO predicted by the model and the results of Keller et al. (reduced mechanism): ◇, NO_x; □, NO_x (Keller); △, CO; and ×, CO (Keller).

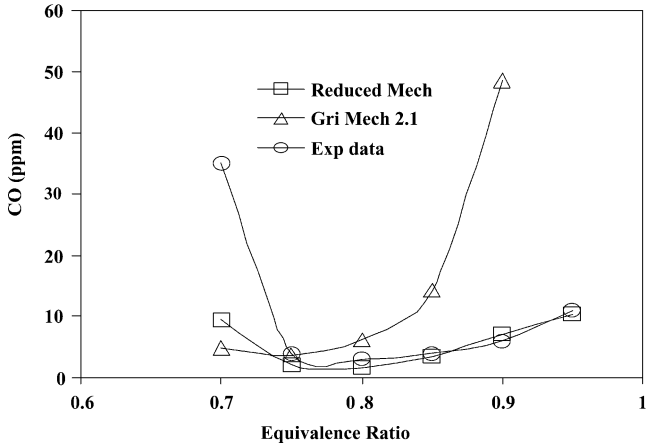

Fig. 11 Comparison of predictions vs data for CO using GRI-Mech. and reduced kinetic mechanism; CO corrected to 3% O_2.

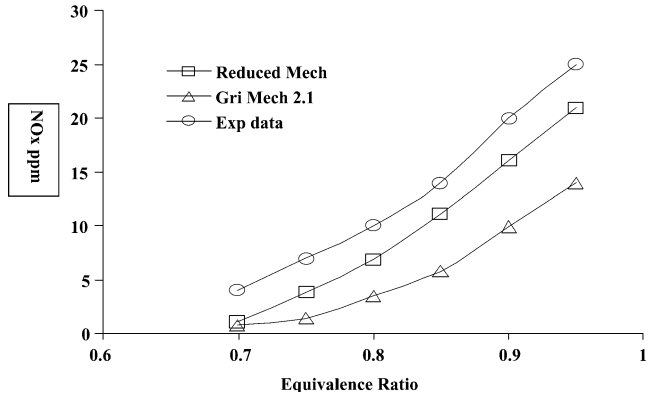

Fig. 12 Comparison of predictions vs data for NO_x using GRI-Mech and reduced kinetic mechanism; NO_x corrected to 3% O_2.

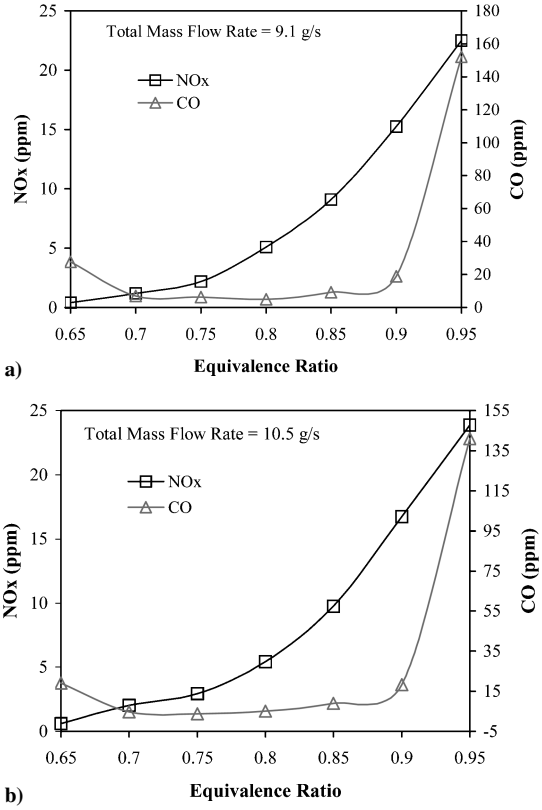

Fig. 13 NO_x and CO (corrected to 3% O_2) as function of equivalence ratio using oscillatory heat transfer coefficient for total mass flow rates of a) 9.1 g/s and b) 10.5 g/s.

equivalence ratio increase. As expected, the values of N_2O increases for decreasing equivalence ratio, also for the reduced model,[16] with reasonable agreement between the two schemes. Again consistent for both models, H_2 values increase for increasing equivalence ratio, resulting from dissociation between the simultaneous presence of O_2, CO, and H_2. By comparison, note, for the reduced scheme,[9] that the hydroxyl radical OH and HCN both peaked at $\phi = 0.9$, before reducing at $\phi = 0.95$. This clearly has implications affecting NO_x and CO formation, especially for equivalence ratios >0.75, shown in Figs. 10–12 and discussed later.

In Fig. 10, predicted time-averaged values of NO_x and CO obtained using the reduced mechanism are compared against the experimental data of Keller et al.[12] CO predictions are in a good agreement with the experimental results, apart from $\phi < 0.74$, whereas NO_x predictions differ from the experimental data by a few parts per million.

Optimal operating conditions in terms of primary pollutant performance can be determined from Figs. 10–12 for both models, as well as the experimental data. At $\phi \sim 0.74$, both NO_x and CO are less than 10 ppm for both models and experiment. Further reduction in equivalence ratio limits the performance in terms of CO, due to the increase in CO emissions that occurs when $\phi > 0.7$, although this characteristic is least prominent for the detailed kinetic mechanism. For ϕ between 0.73 and 0.8, both NO_x and CO emissions are under 10 ppm for all three cases.

The detailed mechanism compares less favorably with the experimental data of Keller et al.[12] than the reduced scheme. GRI-Mech2.11 significantly overpredicts CO for equivalence ratios >0.8 (Fig. 11), whereas the reduced mechanism performs well in the same region. The model using GRI-Mech2.11 underpredicts NO_x (Fig. 12), for all equivalence ratios: The reduced mechanism generally performs better. There are many plausible reasons for this finding, including differences between the experimental setup and

the model assumptions and limitations of the phenomenological approach; however, the most likely explanation arises from that the reduced mechanism is constructed from GRI-Mech3, which contains a more detailed reaction scheme compared to GRI-Mech2.11. Further work is needed to investigate these influences.

Finally, in contrast with the data of Keller et al.,[12] which show that NO_x and CO levels are relatively independent of mass loading, dependency between mass flow and pollutant predictions is observed using a constant Nusselt number, such that increasing the mass loading increased the levels of NO_x and CO levels for all equivalence ratios tested. Figures 13a and 13b show the NO_x and CO concentrations predicted for two different mass flow rates as function of equivalence ratio using the oscillatory Nusselt number introduced earlier. The values of NO_x for both mass flow rates show a monotonically decreasing trend from 24 and 23 ppm, respectively, at $\phi = 0.95$ to 2 and 1 ppm, respectively, at $\phi = 0.7$, that is, consistent with the experimental findings of Keller et al.,[12] CO predictions are relatively insensitive to mass flow rate variation.

V. Conclusions

1) Primary pollutants NO_x and CO have been predicted from a phenomenological pulse combustor model for the first time. The relative simplicity of the thermofluid model employed has the advantage over a more rigorous Navier–Stokes solution in that detailed chemical kinetic models can be readily employed within the integrated model.

2) A detailed kinetic mechanism (GRI-Mech2.11) and reduced mechanism (using 21 species and 17 reactions) have each been coupled with the thermofluid model at each time step, providing two integrated thermal pulse combustor models. The usual oscillatory behavior of pressure and temperature with the addition of combustion species is predicted for both integrated models, hence, facilitating performance comparison.

3) Both integrated models predict pressure, temperature, and the species inside combustor. The results from the combustor were taken as initial conditions to run the model of the tailpipe.

4) Both integrated models predict the characteristic U-shaped CO trend predicting CO < 5 ppm at about $\phi = 0.74$ and increasing as ϕ reduces below 0.7. Both models predict monotonically increasing NO_x with increase in equivalence ratio.

5) An oscillatory Nusselt number is necessary to decouple the dependence of pollutant levels on mass loading found when using a constant Nusselt number, hence, providing predictions consistent with experimental findings.

6) Predictions using the reduced mechanism agree with the experimental data and show low concentrations of CO and NO_x of <10 ppm attained when $\phi = 0.74$. Experimental studies and both models presented now agree that this is the optimal operating range in terms of pollutant performance. However, the CO contribution is very sensitive to further reductions in equivalence ratio, indicating that combustor control is critical in practical lean-burn operation.

7) The results from the reduced mechanism provided better quantitative agreement than those from the detailed mechanism of GRI-Mech2.11 for primary pollutants. The possible reason for this apparent anomaly may arise from the derivation of the reduced mechanism from GRI-Mech3 and mirrors the experiences of other researchers.

References

[1]Zinn, B. T., "Pulse Combustion: Recent Applications and Research Issues," *Proceedings of the Twenty-Fourth Symposium (International) on Combustion*, Combustion Inst., Pittsburgh, PA, 1992, pp. 1297–1305.

[2]Keller, J. O., and Hongo, I., "Pulse Combustion: The Mechanisms of NO_x Production," *Combustion and Flame*, Vol. 80, No. 3–4, 1990, pp. 219–237.

[3]Keller, J. O., Bramlette, T. T., Dec, J. E., and Westbrook, C. K., "Pulse Combustion: The Importance of Characteristic Times," *Combustion and Flame*, Vol. 75, No. 1, 1989, pp. 33–44.

[4]Au-Yeung, H. W., Garner, C. P., and Hanby, V. I., "Modelling the Effects of Combustion Frequency and Pressure Amplitude on NO Formation in a Gas-Fired Combustor," *Journal of the Institute of Energy*, Vol. 72, No. 492, 1999, pp. 70–76.

[5]Au-Yeung, H. W., Garner, C. P., and Hanby, V. I., "Experimental Study of the Effects of Combustion Frequency and Pressure Amplitude on NO Formation from Pulse Combustor," *Journal of the Institute of Energy*, Vol. 71, No. 489, 1998, pp. 204–208.

[6]Richards, G. A., Morris, G. J., Shaw, D. W., Keeley, S. A., and Welter, M. J., "Thermal Pulse Combustion," *Combustion Science and Technology*, Vol. 94, No. 1–6, 1993, pp. 57–85.

[7]Marsano, S., Bowen, P. J., and O'Doherty, T., "Cyclic Modulation Characteristics of Pulse Combustors," *Proceedings of the Twenty-Seventh Symposium (International) on Combustion*, Combustion Inst., Pittsburgh, PA, 1999, pp. 3155–3162.

[8]Marsano, S., "Modelling Transient Combustion Systems," Ph.D. Dissertation, Div. of Mechanical Engineering and Energy Studies, Cardiff Univ., Cardiff, Wales, U.K., 1999.

[9]Sung, C. G., Law, C. K., and Chen, J. Y., "Augmented Reduced Mechanisms for NO Emission in Methane Oxidation," *Combustion and Flame*, Vol. 125, No. 1–2, 2001, pp. 906–919.

[10]Heravi, H. M., Bowen, P. J., Dawson, J. R., and Syred, N., "An Integrated Thermo-Fluid, Chemical Kinetic Model for Pulse Combustors," 42nd AIAA Aerospace Sciences Meeting and Exhibit, Jan. 2004, pp. 9081–9088.

[11]Smith, G. P., Golden, D. M., Frenklach, M., Moriarty, N. W., Eiteneer, B., Goldenberg, M., Bowman, C. T., Hanson, R. K., Song, S., Gardiner, W. C., Jr., Lissianski, V. V., and Qin, Z., http://www.me.berkeley.edu/gri_mech/ [cited 1 Dec. 2003].

[12]Keller, J. O., Bramlette, T. T., Barr, P. K., and Alvarez, J. R., "NO_x and CO Emissions from a Pulse Combustor Operating in a Lean Premixed Mode," *Combustion and Flame*, Vol. 99, 1994, pp. 460–466.

[13]Corliss, J. M., Putnam, A. A., Murphy, M. J., and Locklin, D. W., "NO_x Emissions From Several Pulse Combustors," American Society of Mechanical Engineers, ASME Paper 84-JPGC-APC-2, Dec. 1984.

[14]Barham, P., David, J., Hargreaves, K. J. A., Ipakchi, H., and Maskell, W. C., Sauba, R. N., and Suthenthiran, A., "Characterisation of a 5 kW Gas-Fired Pulsed Combustors: NO_x and CO," *Proceedings of Emissions Control II*, Inst. of Energy, London, 1995, pp. 220–238.

[15]Beale, A. J., "Aerovalved Pulse Combustion," Ph.D. Dissertation, Div. of Mechanical Engineering and Energy Studies, Cardiff Univ., Cardiff, Wales, U.K., 1999.

[16]Heravi, H. M., "Integrated Physical and Chemical Modelling of Pulse Combustors," Ph.D. Dissertation, Div. of Mechanical Engineering and Energy Studies, Cardiff Univ., Cardiff, Wales, U.K., 2003.

[17]Kee, R. J., Rupley, F. M., and Miller, J. A., "ChemkinII: A Fortran Chemical Kinetic Package for the Analysis of Gas Phase Chemical Kinetics," Sandia National Labs. Rept. SAND 89-8009, Livermore, CA, 1989.

[18]Avduevsky, V. S. (ed.), *Heat Transfer Foundation in Aerospace Engineering, Mashinostroenie*, Moscow, 1992, p. 518.